Micro- and nano-structures in silicon studied by DLTS and scanning probe methods

© D. Cavalcoli¶, A. Cavallini, M. Rossi, S. Pizzini*

Physics Dept University of Bologna,
Viale Berti Pichat 6/II, Bologna, Italy
* Material Science Dept University of Milan-Bicocca,
Via Cozzi 53, Milano, Italy

(Получена 12 сентября 2006 г. Принята к печати 3 октября 2006 г.)

Presently there is a high interest in silicon-based optical devices that would render possible the development of fully silicon-based optoelectronics. Being an indirect gap semiconductor, silicon is poorly efficient as light emitter since radiative emission is limited by carrier recombination at non-radiative centers. One of the possible approaches to enhance the radiative emission from Si is the controlled introduction of micro- (dislocations) or nano- (nanocrystals) structures, which, providing quantum confinement of free carriers, prevent their diffusion towards non-radiative channels. Dislocations introduced in silicon by plastic deformation and Si nanocrystals embedded in amorphous silicon matrix have been investigated by junction spectroscopy and scanning probe microscopy methods.

PACS: 61.72.-y, 71.55.Jv, 73.20.Hb, 73.50.Pz

1. Introduction

Light emission from Si is strongly inefficient, as band-to-band optical transitions are highly improbable and most of the excited electron–hole pairs recombine non-radiatively. Nevertheless, there is a strong demand for an optical emitter to be compatible with standard silicon-based ultra-large-scale integration technology. For this reason since 1990 many strategies, reviewed in [1], have been employed to overcome these materials limitations and to obtain efficient light emission from Si. One of the most successful is based on the modification of free carrier properties by quantum confinement effects, firstly obtained by the use of porous Si [2], then by the controlled production of Si nanocrystals in a SiO_2 matrix [3]. Promising results could also be expected by using nanocrystalline hydrogenated Si as it mimics Si dots in a matrix of a-Si characterized by a larger energy gap, and then potentially inducing quantum confinement effects, provided one succeeds in reducing the size of the crystallites to few nm in diameter [4]. Another approach is based on the suppression of non-radiative recombination centers using for the device fabrication high quality substrates and defect passivation procedures [5]. Among the various attempts very recently made in order to increase the efficiency of radiative transitions a significant result was obtained by defect engineering procedures, i. e. by employing dislocations as light emission sources [6]. It was, in fact, demonstrated that using an appropriate impurity gettering process followed by the dislocation passivation one could achieve a large enhancement of the radiative transitions with respect to the non-radiative ones.

For these reasons dislocations, although studied for many years, are still subject of strong interest. One point, which still requires further investigations, is related to dislocation-related shallow bands. Their existence has been predicted by theory and modeling, it has been related with several experimental phenomena [7], but only recently directly observed experimentally by junction spectroscopy [8]. On the contrary, several deep levels are often found to be related to dislocations. Obviously, contamination with transition metals, oxygen precipitation, and impurity–dislocation interaction should play a major role in the dislocation related deep levels formation.

On the contrary, Si nanocrystals in amorphous Si matrix, notwithstanding its high potential for future optoelectronic applications, have not been extensively investigated up to now. It is well known that nanocrystalline silicon (a/nc-Si : H) is considered as a promising candidate for low cost and high efficiency solar cells, having already reached in lab tests top efficiencies around 11%, comparable with those obtained using stabilized amorphous silicon (a-Si) [9]. At the same time its full optoelectronic potentiality is still under investigation, due to the relatively poor knowledge of the correlations between growth conditions, microstructure and physical properties.

As an example of beam-injection methods applied to the study of micro- and nanostructures in silicon, the present paper reports studies, by junction spectroscopies and scanning probe methods, of dislocations introduced in silicon through plastic deformation and Si nanocrystals embedded in amorphous Si matrix.

The results relevant to the investigation of dislocations in Si were published in previous papers [8,10], and here reviewed. The analyses of dislocations introduced in different Si wafers (with low and high O content) and with different procedures (plastic deformation and oxygen precipitation) have allowed us to clarify the effect of metallic contamination and oxygen precipitation on states related to extended defects, the presence of dislocation-related shallow bands and the characteristics of the dislocation-related deep states in p-type Si.

¶ E-mail: cavalcoli@bo.infn.it

Moreover, nanocrystals embedded in amorphous Si matrix were investigated by C-AFM (conductive atomic force microscopy) and SPS (surface photovoltage spectroscopy). C-AFM allowed us for detailed analyses of the conduction mechanisms within this complex multi-phase material, while SPS allowed for determination of the optical band gap and defect states.

2. Experimentals

2.1. Investigation of dislocations

Several Si samples have been investigated in order to distinguish between the different factors (dislocations, impurities, point defects) contributing to the defect states.

1) As-grown p-type (B-doped, $[B] = 1.6 \cdot 10^{16}\,cm^{-3}$) Cz-Si (czochralski technique) containing interstitial O and/or unintentionally contaminated by grown-in metals.

2) Oxygen precipitated Si (containing oxygen precipitates and punch-out-dislocation, set OXP).

3) Plastically deformed Cz-Si containing dislocations and deformation-induced point defect clusters (set Cz-1).

4) Plastically deformed Cz-Si containing straight, 60° dislocations and O-segregated 60° dislocations (set Cz-0). The samples were ad hoc prepared in order to obtain a regular array of parallel 60° segments (DD). The dislocated samples were then annealed at 800°C for 24 h in argon (DDTT).

5) Plastically deformed float zone Si (Fz-Si) containing dislocations in a low O-content matrix (set Fz-1).

Further details of the deformation procedure and of the obtained dislocation systems are reported in [10], the material characteristics are summarized in Table 1.

The samples were investigated by deep level transient spectroscopy (DLTS) and minority carrier transient spectroscopy (MCTS) [8,10].

Table 1. Labels and characteristics of the Si samples

Sample set	Samples	Treatment
OXP (p-type)	#62	15 min preannealing at 1000°C nucleation: 4 h at 800°C growth: 4 h at 800°C + 4 h at 1000°C
	#87	15 min preannealing at 1000°C nucleation: 64 h at 800°C growth: 4 h at 800°C + 16 h at 1000°C
Cz-1 (p-type)	Cz-AG Cz-H Cz-DEF	As grown Heated at 670°C for 1 h in argon Deformed at 670°C for 1 h in argon
Cz-0 (p-type)	W DD DDTT	As grown Deformed by 2-step procedure Deformed as DD + annealing for 24 h at 800°C in argon
Fz-1 (n-type)	Fz-AG Fz-DEF	As grown Deformed at 670°C for 1 h in argon

2.2. Investigation of Si nanocrystals

Nanocrystalline hydrogenated Si films (a/nc-Si H) were grown on oxidized crystalline silicon substrates by the low-energy plasma enhanced chemical vapour deposition (LEPECVD) process, which was shown to present the advantage over other PECVD techniques to get higher growth rates and better surface and subsurface properties, due to lower ion implantation damage [11]. The films were deposited on oxydized Si in the temperature range 400−200°C, using SiH_4 and H_2 flows leading to silane dilution ratios $d = \Phi(SiH_4)/[\Phi(SiH_4) + \Phi(H_2)]$ ranging between $d = 1.96$ and 5.6%, always well below the a-Si/nc-Si phase transition, which is expected at d values around 25%. The growth rate obtained ranged between 0.5 and 1.3 nm/s [11].

The samples have been investigated by C-AFM and SPS. C-AFM analyses have been carried out using an AFM system by NT-MDT (model Solver PRO) in contact mode with a Pt coated probe: by applying a constant bias to the AFM tip and grounding the sample, high resolution current maps have been obtained. SPS analyses were performed by a lab-made apparatus based on a SPEX 500M monochromator [12], the system allows for the measurement of surface photovoltage (SPV) signal in wide spectral range (300−2000 nm) by the use of different gratings and light sources (quartz-tungsten-halogen and xenon).

3. Results

3.1. Investigation of dislocations by junction spectroscopy

DLTS analyses of plastically deformed and thermally treated crystalline silicon showed the presence of several deep levels. Their characteristics are reported in the followings.

Deep hole traps in OXP, Cz-1 *and* Fz-1 *sets.* Four hole deep traps, named T1, T2, T3, T4, have been detected by DLTS in the p-type samples of OXP and Cz-1 sets and by MCTS in the n-type samples of Fz-1 set. As some of the DLTS peaks are broadened, they should be analysed with the appropriate model [7] instead of the procedure used to analyse point-like defects. However, for the sake of comparison with literature data, the T^2-corrected thermal emission rates e_p relevant to the different samples are presented in Figs 1 and 2 as a function of the inverse temperature $1/T$. The trap characteristics (apparent activation energy and capture cross-sections as evaluated by the Arrhenius plot) are reported in the figure captions. In details: T1, T2 and T3 traps were detected in OXP set (Fig. 1), T1, T3 and T4 in Cz-1 and Fz-1 sets (Fig. 2). The relevant Arrhenius plots have been compared in Figs 1 and 2 with literature results relevant to hole traps detected in: plastically deformed (Fz) Si [13] and O-precipitated Si [14], and with the interstitial iron trap in Si [15]. Trap T3

results from two different contributions [10]: T3a, present only in the as-grown samples, and T3b, which is present in thermally treated samples. These traps correspond to grown-in iron in different configuration: Fe_i in as-grown samples (W), where the shallow trap T0, related to the FeB pair is also detected [8] and the Fe–O complex in thermally treated samples (DD, DDTT).

Deep hole traps in Cz-0 *set.* The three traps (T1, T2 and T3) have been detected in these samples (Fig. 3). As in the previous case, T3 is made up by the two different contributions T3a and T3b. T2, found only in DD, whose Arrhenius plot is in good agreement with the one of traps H(.49) [13], corresponds to a broad and asymmetric peak in the DLTS spectra and is not detected in the annealed samples DDTT. The same line has been found also in oxygen precipitated Si [14] and attributed to point defect centers not localized at dislocations. The line T1, found in DDTT, could correspond to the level H.33 [13], found in plastically deformed Si and often related to impurities in the dislocation strain field.

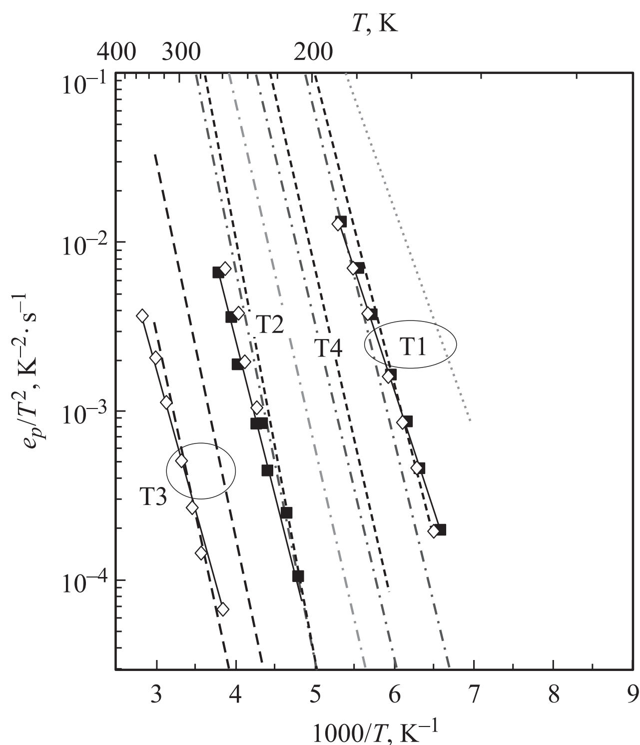

Figure 1. T^2-corrected thermal emission rates of the traps T1, T2 and T3 found in the OXP set. Points are the present experimental data, solid lines are the data best fit, dashed and dotted lines represent literature data. Filled squares (#62), open diamonds (#87); dashed lines: the interstitial iron related levels; dotted lines: traps P1 (short dot) and P2 (short dash-dot) [14]; traps H(.33) and H(.49) [13] (short dashed lines). Trap parameters (activation enthalpy E_T, eV / capture cross section σ, cm^2) as evaluated by the Arrhenius plot are as follows: T1 $(0.27-0.28)/(10^{-15}-10^{-16})$; T2 $(0.42-0.45)/10^{-15}$; T3 $0.40/10^{-17}$.
Reproduced from Appl. Phys. Lett., **86**, 162 109 (2005). Copyright 2005, American Institute of Physics.

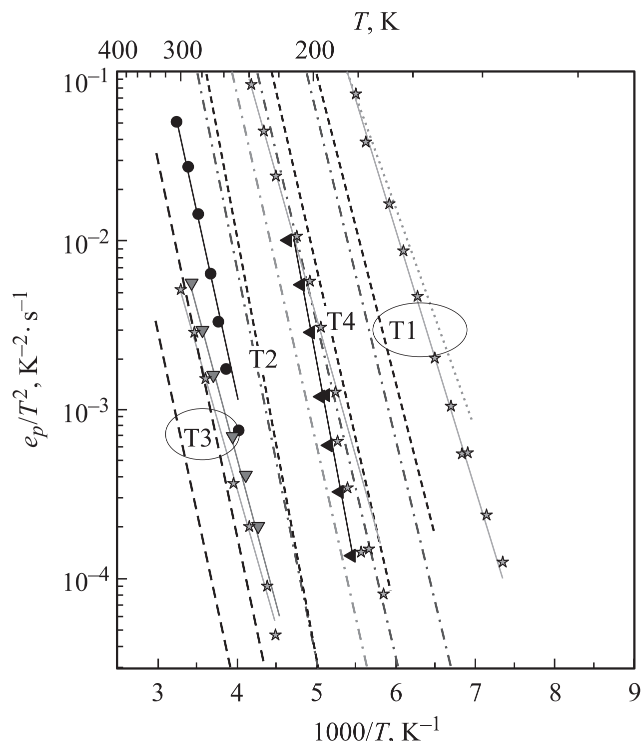

Figure 2. T^2-corrected thermal emission rates of the traps T1, T2, T3 (a, b) and T4 in the Cz-1 and Fz-1 sets. Circle (Cz-AG), down triangle (Cz-H), star (Cz-DEF), left triangle (Fz-DEF). Literature data have been plotted simularly to that in Fig. 1. Trap parameters of T4: $E_T = 0.38$ eV, $\sigma = 10^{-15}$ cm^2.
Reproduced from Appl. Phys. Lett., **86**, 162 109 (2005). Copyright 2005, American Institute of Physics.

Shallow traps in Cz-0 *set.* Two shallow hole traps, labeled T0 and STh [10], have been detected. The former, T0, has the same signature as the FeB pair [14], is detected only in as-grown samples (W) where T3a (Fe_i) is also detected. Thus it can be related to the FeB pair. The latter is a shallow hole trap located at $E_v + 70$ meV, which appears only after annealing. The trap is detected only when the DLTS spectrum is measured in a dislocation area of the sample (Fig. 4). In these samples a shallow trap for minority carriers (electrons), labeled STe, has also been detected by MCTS [10]. As Fe is ubiquitously present in these samples, to a first guess STh and T0 could both be related to the FeB pair that introduces in Si a level located around 0.1 eV from the valence band edge [14]. A photo-dissociation experiment showed that STh is not related to the iron–boron pairs [8]. The capture kinetics of STh studied by DLTS [8] showed that this trap is associated with a repulsive Coulomb potential.

3.2. Investigation of Si nanocrystals

Morphological properties of nc-Si:H films grown by LEPECVD were analysed by AFM topography maps (Fig. 5). The films presented the expected columnar

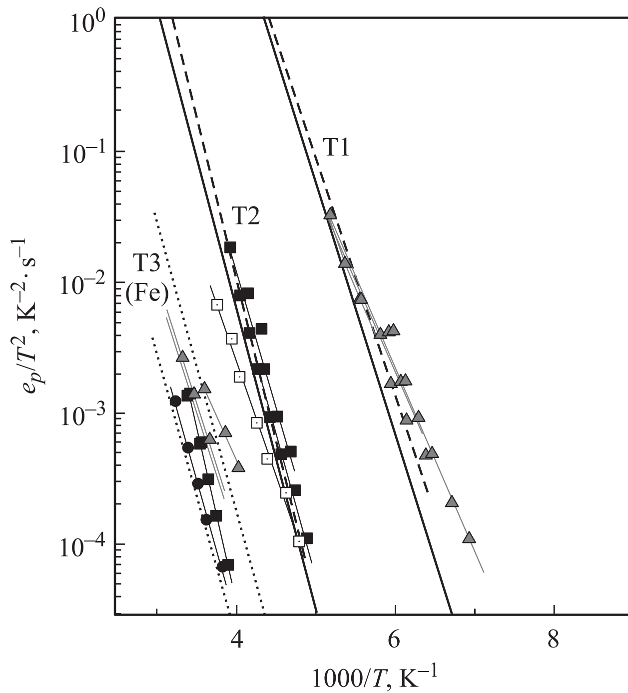

Figure 3. T^2-corrected thermal emission rates as a function of inverse temperature for the DLTS lines T1, T2, T3 and STh found in the Cz-0 set (circles), DD (squares), DDTT (triangles). Thin solid lines represent data fitting. Literature data (thick lines) from: [13] (dashed lines), [14] (dotted lines) and [8] (open squares) are also reported.
Reproduced from: Defects and Diffusion Forum, **245–246** (2005), p. 15. Copyright 2005 Trans. Tech. Publications, Switzerland.

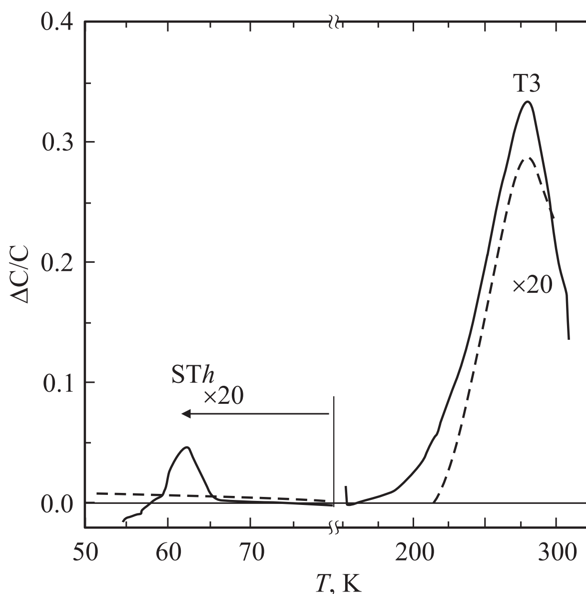

Figure 4. DLTS spectra of one sample of the set DDTT. Rate window 46 s^{-1}, bias 3, 0, −3 V, filling pulse 1 ms. Dashed line: spectrum far away from dislocations, solid line: spectrum in the close proximity of dislocations. At this value of the rate window trap T1 is masked by T3.
Reproduced from: Defects and Diffusion Forum, **245–246** (2005), p. 15. Copyright 2005 Trans. Tech. Publications, Switzerland.

structure [16]: the surface morphology of the films shows the „head“ of such columns. The section of each column will be labeled from now as „domain“. It is widely accepted that these disordered phases are favourable locations for hydrogen and dangling bonds [16] and thus are reminiscent of amorphous silicon. The crystalline columns have typical widths of 50−200 nm and are far from perfectly grown single crystals. They contain a large number of imperfections like dislocations, stacking faults and tilt boundaries. The electrical properties of this complex multiphase material are difficult to understand, in this respect microscopical electrical measurements are a valuable tool to understand the conduction mechanisms. An example of a C-AFM map of a/nc-Si : H film is shown in Fig. 6. It can be noted the strong inhomogeneity at a microscopic level of the material: the current (which at constant bias is related to the conductivity) lower in the core than at the boundary of each domain, as shown also in Fig. 6, inset.

Surface photovoltage spectroscopy [17] is a valuable tool for the investigation of optical properties of semiconductors, as the surface photovoltage is proportional to the absorption coefficient. From SPS spectra the optical gap can be evaluated as from optical absorption spectra, with the advantage that the measurement is non-contact and non-destructive, it does not need any sample preparation. In a/nc-Si : H where different phases (amorphous and crystalline) coexist and large defect concentrations are possibly present, significant

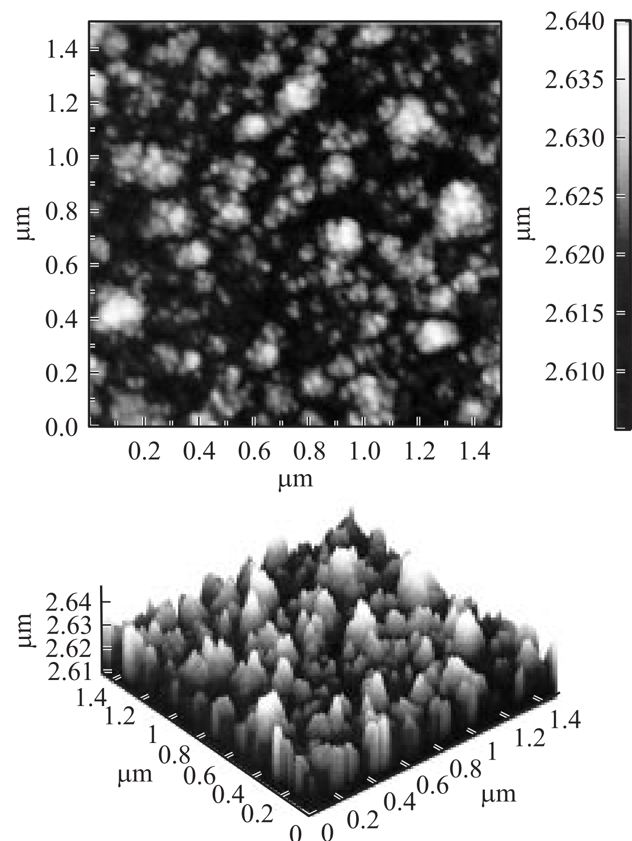

Figure 5. Atomic force microscopy map of the a/nc-Si : H film grown at 210°C, with the rate of 0.12 nm/s, dilution factor 4.2%.

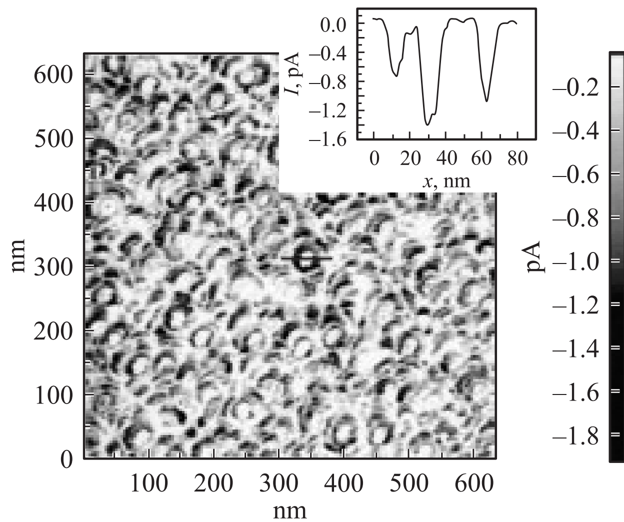

Figure 6. C-AFM current map with bias voltage of 3.5 V, of the a/nc-Si:H film grown at 235°C, with rate of 0.95 nm/s, dilution factor 4.2%. In the inset, the current profile $I(x)$ across one single domain is shown.

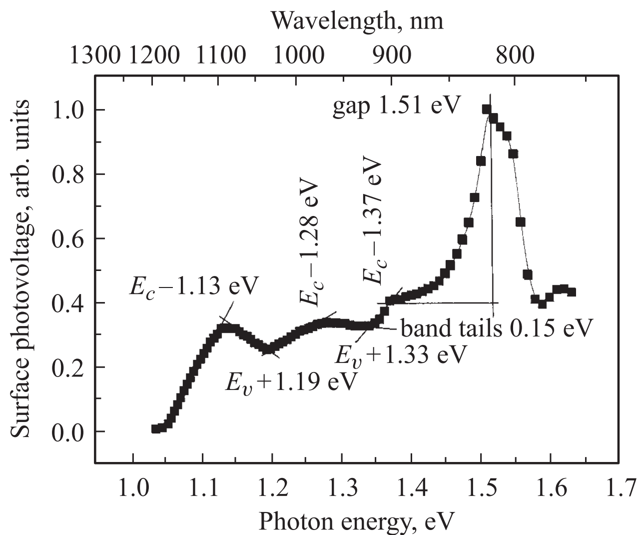

Figure 7. Surface photovoltage spectrum of the a/nc-Si:H film grown at 235°C, with the rate of 0.95 nm/s, dilution factor 4.2%. Electron transitions from–to conduction and valence bands are shown.

absorption by subband gap states contributes to the SPV signal, thus the usual extrapolation procedure to get the band gap can not be used. The band gap energy [18] was determined via the identification of the band-gap related „knee“ energy. An example is shown in Fig. 7: the a/nc-Si:H band gap is around 1.5 eV, comparable with literature values relevant to similar material [19].

SPS analyses carried out with below band gap light allow for defect state spectroscopy (Fig. 7). Bulk-, as well as surface-related electronic transitions can be detected [17]: in n-type material each decrease of the surface potential is related to depopulation of gap states (electron transition from the gap state to the conduction band) while each increase to population of gap states (electron transition from the valence band to the conduction band). The obtained electron transitions are shown in Fig. 7.

4. Discussion and conclusion

Beam injection methods applied to dislocations and nanocrystals in Si were valuable tools for the knowledge of material properties, in view of their applications as active device in Si-based optoelectronics. DLTS studies of crystalline Si has allowed us for a detailed analysis of the different factors contributing to the dislocation-related deep states. The following conclusions can be drawn. Cz-Si, as-grown, heated, deformed or oxide precipitated, contains a detectable amount of grown-in Fe, that can form complexes with O during thermal treatments. Trap T3, detected in almost all the samples investigated is due to Fe contamination. Oxygen precipitates induce two hole deep traps: T1 related to impurities in the strain field of extended defects (dislocations or O precipitates) and T2 related to defect centers at Si/SiO_2 interfaces. Plastic deformation induces several traps, mainly related to deformation-induced point defects. The main deep trap that survives after high temperature annealing, and is likely related to dislocations, is T1. T1 is detected also in oxygen-precipitated samples and it could be related to localized states at extended defects. A similar trap (but thermally unstable) is observed also in Fz-Si [13]. We believe that O precipitation should play an important role in the thermal stability of trap T1. Dislocations, besides deep traps, induce shallow bands, always predicted by theory and modeling, observed experimentally in [8] as shallow localized states (STe and STh). These two shallow traps were observed after the annealing procedure, which caused O segregation at dislocations. O segregation changed the structural, and consequently the electrical properties of the dislocations in such a way that these states become detectable by DLTS. Moreover, O precipitation causes a modification of the strain field in proximity of dislocations that can change the characteristics of the DLTS spectrum from band-like to localized [8].

C-AFM and SPS analyses of a/nc-Si:H films showed to be very valuable tool for the knowledge of conduction mechanisms and the defect states in a/nc-Si:H films. First of all, by C-AFM analyses, a tentative hypothesis on the conduction mechanism through the film can be advanced: as the conductivity increases at the boundaries between columns, conduction could occur via a percolation mechanism along the disorder tissue between such columns. This hypothesis is also confirmed by literature data [20]. Moreover, SPS analyses allowed for the determination of the optical band gap of the film, and for the determination of the electron transitions at defect states in the gap.

This work was carried out in the frame of two EU-founded Research Projects: the DEDALES INTAS contract 2000-0194 and the „NANOPHOTO“ (VI Framework Program) project contract 013944. All the project partners are gratefully acknowledged.

References

[1] L. Pavesi. J. Phys. Condens. Matter, **15**, R1169 (2003).
[2] L.T. Canham. Appl. Phys. Lett., **57**, 1046 (1990).
[3] L. Pavesi, L. Dal Negro, C. Mazzoleni, G. Franzò, F. Priolo. Nature, **408**, 440 (2000).
[4] S. Pizzini, M. Acciarri, S. Binetti, D. Cavallini, D. Chrastina, L. Colombo, E. Grilli, G. Isella, M. Lancin et al. Mater. Sci. Eng. B, (2006) in press.
[5] M.A. Green, J. Zhao, J.A. Wang, P.J. Reece, M. Gal. Nature, **412**, 805 (2001).
[6] V. Kveder, M. Badylevich, E. Steinman, A. Izotov, M. Seibt, W. Schröter. Appl. Phys. Lett., **84**, 2106 (2004).
[7] W. Schröter, H. Cerva. In: *Defect Interaction and Clustering* (Trans Tech, Zürich, 2001).
[8] A. Castaldini, D. Cavalcoli, A. Cavallini, S. Pizzini. Phys. Rev. Lett., **95**, 76401 (2005).
[9] A. Shah, J. Meier, E. Vallat-Sauvain, C. Droz, U. Kroll, N. Wyrsch, J. Guillet, U. Graf. Thin Sol. Films, **403**–**404**, 179 (2002).
[10] A. Castaldini, D. Cavalcoli, A. Cavallini, S. Binetti, S. Pizzini. Appl. Phys. Lett., **86**, 162 109 (2005).
[11] S. Binetti, M. Acciarri, M. Bollani, L. Fumagalli, H. von Känel, S. Pizzini. Thin Sol. Films, **487**, 19 (2005).
[12] D. Cavalcoli, A. Cavallini, M. Rossi. J. Electrochem. Soc., **151**, G248 (2004).
[13] C. Kisielowski, E.R. Weber. Phys. Rev. B, **44**, 1600 (1991).
[14] T. Mchedlidze, K. Matsumoto, E. Asano. Jap. J. Appl. Phys., **6A**, 3426 (1999).
[15] A.A. Istratov, H. Hieslmair, E.R. Weber. Appl. Phys. A, **69**, 13 (1999).
[16] K. Lips, P. Kanschat, W. Fuhs. Sol. Energy Mater. Solar Cells, **78**, 513 (2003).
[17] L. Kronik, Y. Shapira. Surf. Interface Anal., **31**, 954 (2001).
[18] D. Gal, Y. Mastai, G. Hodes, L. Kronik. J. Appl. Phys., **86**, 5573 (1999).
[19] S. Gupta, G. Morell, B.R. Weiner. J. Non-Cryst. Sol., **343**, 131 (2004).
[20] B. Rezek, J. Stuchlik, A. Fejfar, J. Kocka. J. Appl. Phys., **92**, 587 (2002).

Редактор Л.В. Шаронова